

## Article

# Flexoelectric Polarization in Liquid Crystalline Elastomers Prepared by Cross-Linking under Horseshoe-Shaped Deformation

Kazuyuki Hiraoka \*, Toshio Ishihara, Hiroyuki Minami, Shiori Taira, Katsumi Yamada and Toshihiro Hiejima

Department of Life Science &amp; Sustainable Chemistry, Tokyo Polytechnic University, 1583 Iiyama, Atsugi-shi 243-0297, Japan

\* Correspondence: hiraoka@t-kougei.ac.jp

**Abstract:** Flexoelectric polarization, which is caused by symmetry breaking in a distortion of material, was investigated in liquid crystalline elastomers composed of wedge-shaped mesogens prepared by cross-linking under horseshoe-shaped deformation. X-ray diffractometry suggested that splay distortion along the depth direction was induced in the pseudo-isotropic phase. While almost no electric charge was observed in the smectic A phase, an electric charge caused by polarization due to the flexoelectric effect appeared and reached  $-1367 \text{ pC/mm}^2$  in the pseudo-isotropic phase. We tentatively conclude that the macroscopic polarization due to the flexoelectric effect emerged and was fixed in the liquid crystalline elastomers by cross-linking under horseshoe-shaped deformation.

**Keywords:** cross-linked structure; cross section; flexoelectricity; liquid crystalline elastomers; splay; spontaneous polarization



**Citation:** Hiraoka, K.; Ishihara, T.; Minami, H.; Taira, S.; Yamada, K.; Hiejima, T. Flexoelectric Polarization in Liquid Crystalline Elastomers Prepared by Cross-Linking under Horseshoe-Shaped Deformation. *Symmetry* **2023**, *15*, 616. <https://doi.org/10.3390/sym15030616>

Academic Editor: P. Ulrich Biedermann

Received: 10 January 2023

Revised: 13 February 2023

Accepted: 20 February 2023

Published: 1 March 2023



**Copyright:** © 2023 by the authors. Licensee MDPI, Basel, Switzerland. This article is an open access article distributed under the terms and conditions of the Creative Commons Attribution (CC BY) license (<https://creativecommons.org/licenses/by/4.0/>).

## 1. Introduction

Liquid crystalline elastomers have been attracting increasing attention as a novel class of liquid crystalline materials because they give rise to new macroscopic features in soft solids with the anisotropic properties of a liquid crystalline phases [1–9]. In particular, they have attracted both scientific and industrial interest as ideal materials for the investigation of piezoelectric and flexoelectric effects, because the polymer network prevents macroscopic flow, which inhibits the emergence of piezoelectricity and flexoelectricity in conventional low-molar-mass liquid crystals. To date, several research groups have demonstrated the mechanical response to electric stimulation attributable to the inverse piezoelectric effect in chiral smectic elastomers, focusing on their potential applications as electrically controllable soft actuators [10–18].

Flexoelectricity, which is associated with the emergence of polarization caused by symmetry breaking by a distortion of material, in liquid crystals as well as liquid crystalline elastomers has been examined in several studies since Meyer predicted its emergence [19–28]. Patel and Meyer [21] and Rudquist et al. [22] pointed out that a periodic splay-bend pattern in the helix of cholesteric liquid crystal couples flexoelectrically to the electric field. Popova et al. reported nonlinear electromechanical coupling due to a local flexoelectric effect in chiral smectic liquid crystals [23]. Meyer et al. [24] predicted and demonstrated an electroclinic effect due to the flexoelectricity in the twist-bend nematic phase. Sreenilayam et al. [25] quantitatively estimated the magnitude of the flexoelectric polarization in bent-core nematic liquid crystals. In addition, flexoelectricity in liquid crystalline elastomers has gained increasing attention since the report of giant flexoelectricity in bent-core nematic liquid crystalline elastomers by Harden et al. [26]. Recently, Hiraoka et al. have reported that the macroscopic polarization due to the flexoelectric effect emerges and is fixed in the liquid crystalline elastomers composed of wedge-shaped mesogens by cross-linking under uniaxial deformation with splay distortion [27]. In addition, they observed an electric field-induced polar deformation resembling the motion of the flukes of a dolphin in the liquid crystalline elastomer [28,29].

In this study, the polarization due to the flexoelectric effect is investigated in liquid crystalline elastomers composed of wedge-shaped mesogens prepared by cross-linking under horseshoe-shaped deformation. X-ray measurements of the cross-section of the elastomer film revealed that the director uniformly aligns parallel to the surface in the vicinity of the surface, while it partially inclines 65 degrees to the surface inside the elastomer film. Although no polarization is observed in the smectic A (SmA) phase, it is detected in the pseudo-isotropic phase in which the orientational order partially remains. Here, smectic liquid crystal phases have a layer structure. In the case of the smectic A (SmA) phase, inside the layers the molecules are parallel, on an average, one to each other with their long axes perpendicular to the layer plane [20]. The emergence of polarization suggests that the splay distortion along the depth direction is induced through the transformation from the SmA phase to the pseudo-isotropic phase. The electric charge due to the polarization increases with the temperature in the pseudo-isotropic phase, reaching  $-1367 \text{ pC/mm}^2$ . We confirm that the macroscopic polarization due to the flexoelectric effect emerges and is fixed in the liquid crystalline elastomers by cross-linking under horseshoe-shaped deformation. The liquid crystal elastomers possessing the spontaneous polarization are suitable for their applications as electrically controllable soft actuators.

## 2. Materials and Methods

An elastomer was synthesized by a hydrosilylation reaction of liquid crystalline side groups with a polysiloxane backbone via a well-known synthesis route [1]. Polymethylhydrosiloxane (polymerization degree of 25–35), undecylenic acid cholesteryl ester, and undecylenic acid 4-undec-10-enyloxy-phenyl ester were used as the polymer backbone, mesogenic monomer, and cross-linker, respectively. Their chemical structures are shown in Figure 1a. It is noteworthy that the cholesterol-derived mesogen seems to be a wedge-shaped molecule (Figure 1b). As previously reported, the electric dipole moment  $p_i$  along the molecular long axis of the cholesterol-derived mesogen was estimated to be about 1.1 D by calculation after the conformational structure of the mesogen was optimized by the semiempirical molecular orbital method [27,29,30]. Wedge-shaped molecules carrying permanent dipole moments, such as the cholesterol-derived mesogens used here, yield macroscopic polarization  $P \neq 0$  when splay distortion is imposed [19,20].

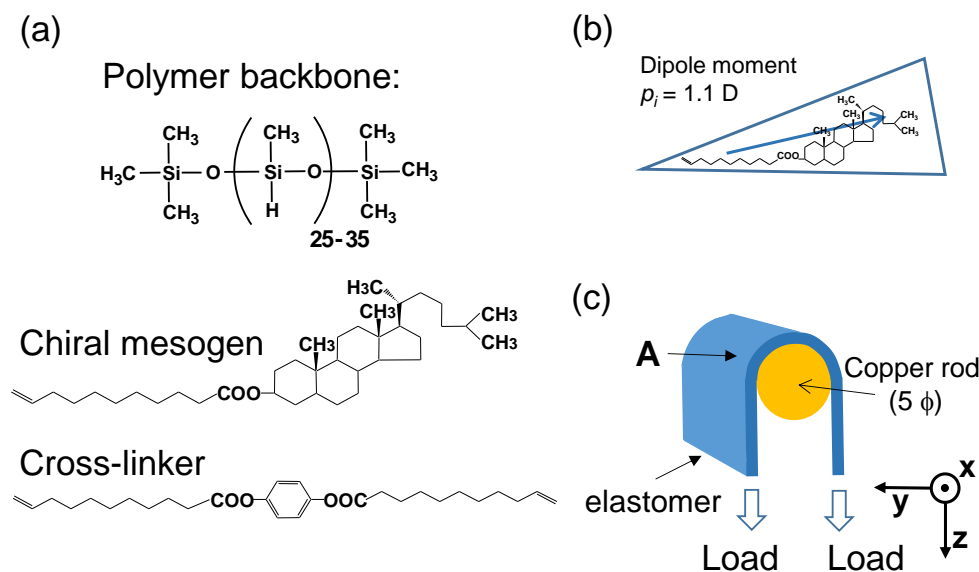


**Figure 1.** System used for investigation. (a) Chemical structures of polymer backbone, cholesterol-derived mesogen, and cross-linker. (b) The cholesterol-derived mesogen is a wedge-shaped molecule. The arrow indicates the direction of electric dipole moment. (c) Sample preparation of a horseshoe-like deformed liquid crystalline elastomer.

The elastomer exhibited the following phase sequence [glassy state 25 °C smectic A phase 110 °C pseudo-isotropic phase] upon heating. As already reported, these transition temperatures were determined by differential scanning calorimetry (DSC), thermomechanical analysis (TMA), and temperature-dependent X-ray diffractometry [27–29]. Because X-ray diffractometry has revealed that the orientational order partially remained at about  $S = 0.2$ , even in the temperature region of the isotropic phase of the liquid crystalline elastomers, as described in previous papers, the temperature region of the isotropic phase here is designated as the pseudo-isotropic phase in this report [27–29,31,32].

The elastomer film was prepared by a spin-casting technique in a solution containing the polysiloxane (2 mmol), the mesogen (1.6 mmol), the cross-linker (0.2 mmol), and a Pt catalyst [platinum (0)-1,3-divinyl-1,1,3,3-tetramethyl-disiloxane complex, Aldrich] in 2 mL of toluene. The reaction was performed under centrifugation (6000 rpm) at 40 °C for 4 h. Thereafter, the reaction vessel was cooled to room temperature and the elastomer, which was swollen with toluene, was carefully removed from the vessel. To obtain a splay distortion of the director, the swollen elastomer is deformed into a horseshoe shape by loading it with a stress of 89.5 mN/mm<sup>2</sup> for 24 h at room temperature, as shown in Figure 1c, in which the loading direction is indicated by a pair of arrows. During the deformation process at room temperature (25 °C), the toluene evaporated continuously from the network, and successive phase transformations occurred from the isotropic phase of the gel to the liquid crystalline phase of the dry network during the sample preparation. Since the cross-linking reaction simultaneously proceeds in the deformation process, the anisotropic orientation of the director in the horseshoe-shaped deformation is chemically locked in the polymer network.

The electric charge was measured using a charge meter (Kistler, Charge meter type 5015) by contacting the tip of a hand-made electrode assembled with a crocodile clip to the surface of a sample at the position marked by arrow A in Figure 1c. The contact area was estimated to be about 1.5 mm<sup>2</sup>. The sample was placed on a temperature-controlled hot plate.

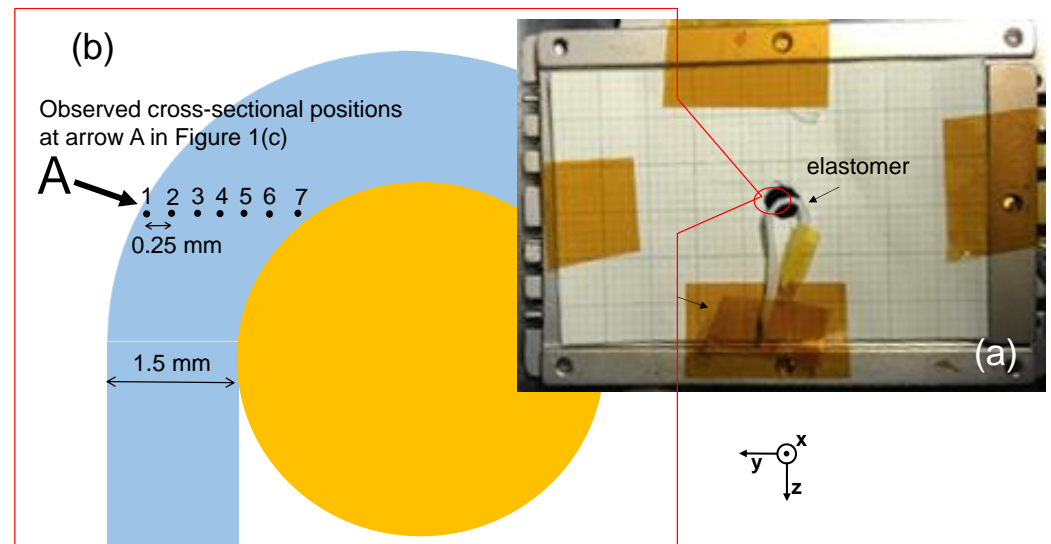
The molecular alignment and orientation in the horseshoe-shaped part of the deformed elastomer [arrow A in Figure 1c] were confirmed by X-ray diffractometry (Rigaku, Nanowier + Micro07HFM using a Cu-K<sub>α</sub> beam filtered by a confocal mirror. X-ray wavelength = 1.54 Å, X-ray power = 2.7 kW). The X-ray beam was narrowed by passing it through a slit (0.4 mm  $\phi$ ). The X-ray measurements were performed using a two-dimensional hybrid pixel array detector (Rigaku Oxford Diffraction, PILATUS200K). The X-rays scattered on the  $y$ - $z$  plane were measured after maintaining the measurement temperature for at least 10 min. The sample was mounted in a microfurnace (Mettler, FP82HT) during the X-ray measurements.

### 3. Results and Discussion

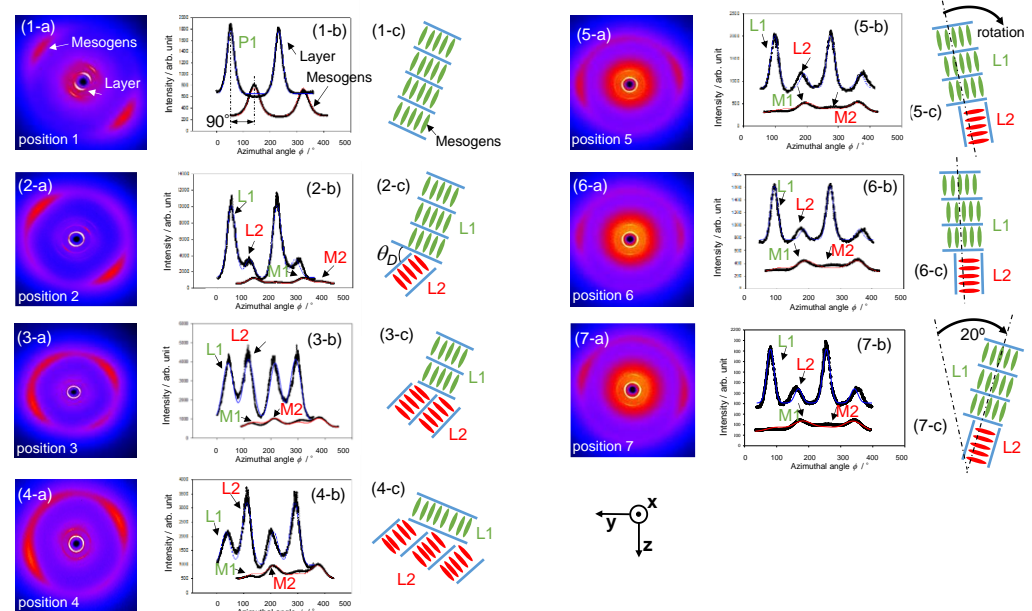
X-ray diffractometry was performed at seven positions to investigate the cross-sectional profile of the macroscopic orientation of the director in the horseshoe-like deformed part of the elastomer at the arrow A position in Figure 1c. Figure 2a shows a photograph of the cross-section of the sample. The observed seven positions are designated consecutively from position 1 to position 7, as illustrated in Figure 2b. Position 1 is nearest the outer surface and position 7 is nearest the inner surface. Position 4 is located near the center of the depth profile. The places of position 5 and the position 6 are shown in Figure 2b. Here, the interval between positions is 0.25 mm and the sample thickness is about 1.5 mm.

Figure 3 shows the results of a series of X-ray analyses at these seven positions. The X-ray measurements were performed at room temperature. Figure 3(1-a)–(1-c) show the X-ray diffraction pattern, the azimuthal X-ray intensity profile, and the molecular orientational model based on the X-ray results at position 1, respectively. As similarly reported in previous papers on uniaxially deformed elastomers [27–29], the orthogonal alignment due to the SmA structure is confirmed by the X-ray diffraction pattern in Figure 3(1-a), in which the small-angle reflections due to the smectic layers and the wide-angle diffrac-

tions associated with the molecular arrangement of the mesogenic side groups within the smectic layers exist. From the analysis of the azimuthal intensity profile of the wide-angle diffraction shown in Figure 3(1-b), we estimate the macroscopic order parameter as  $S = (1/2) \langle 3\cos^2\alpha - 1 \rangle = 0.83$  [33]. The two characteristic reflections indicate that the mesogens and smectic layers are macroscopically uniformly aligned near the surface at position 1, as illustrated in Figure 3(1-c). Compared with the cross-sectional image in Figure 2b, the direction of the director in Figure 3(1-c) seems to be almost parallel to the sample surface.



**Figure 2.** (a) Photograph of cross-section of the sample. (b) The seven positions observed by X-ray diffraction are designated consecutively from position 1 to position 7 as schematically shown.



**Figure 3.** X-ray analysis of seven positions in cross-section of horseshoe-shaped part of deformed liquid crystalline elastomer. X-ray diffraction patterns are shown in (1-a)–(7-a), azimuthal X-ray intensity profiles are shown in (1-b)–(7-b), and molecular orientational models based on X-ray results are shown in (1-c)–(7-c).

Figure 3(2-a)–(2-c) show the X-ray diffraction pattern, the azimuthal intensity profile, and the molecular orientational model at position 2, respectively. The small-angle reflections due to smectic layers and the wide-angle diffractions associated with the mesogenic side

groups are also recognized in Figure 3(2-a),(2-b). It is noteworthy that two peaks are observed in the azimuthal profile of layer reflection at a small angle (L1 and L2) and mesogenic diffraction at a wide angle (M1 and M2) in Figure 3(2-b). The azimuthal profile with two peaks indicates that two smectic domains exist. From the intensity ratio of peak L1 to peak L2 in Figure 3(2-b), the volume ratio of two smectic domains can be estimated to be 3:1, as illustrated in Figure 3(2-c). The X-ray analysis of the larger domain due to peak L1 indicates that the direction of the director seems to be almost parallel to the sample surface, the same as the director at position 1, while the director of another smaller domain due to peak L2 inclines at about  $q_D$  degrees to the director of the larger domain parallel to the surface. In addition, angle  $q_D$  between the two domains is estimated to be about 65 degrees.

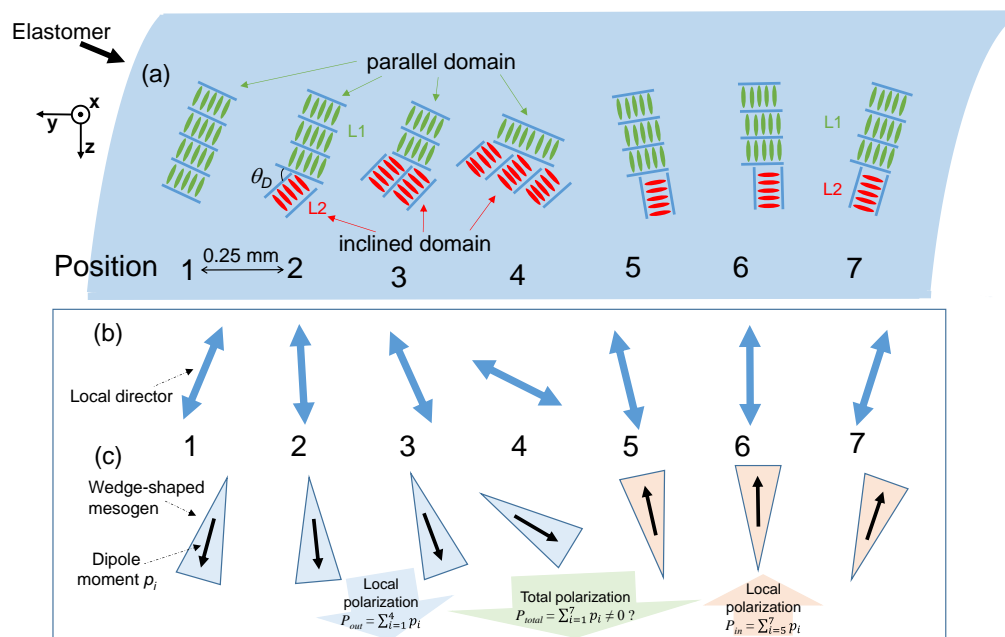
Figure 3(3-a)–(3-c) show the X-ray pattern, the azimuthal profile, and the molecular orientational model at position 3, respectively. Two peaks are also observed in the azimuthal profile of layer reflection (L1 and L2) and mesogenic diffraction (M1 and M2) in Figure 3(3-b). The intensity of peak L1 is almost the same as that of peak L2 in the azimuthal profile in Figure 3(2-b). This means that the volume ratio of two smectic domains can be estimated as 1:1 (=2:2) at position 3, as illustrated in Figure 3(3-c).

Figure 3(4-a)–(4-c) show the X-ray results at position 4 near the center of the depth profile. Two peaks are also observed in the azimuthal profile of layer reflection (L1 and L2) and mesogenic diffraction (M1 and M2) in Figure 3(4-b). The intensity of peak L2 becomes higher than that of peak L1 at position 4. From the peak intensity ratio between peak L1 and peak L2 in Figure 3(4-b), the volume ratio of two smectic domains is estimated to be 1:3, as illustrated in Figure 3(4-c).

Figure 3(7-a)–(7-c) show the X-ray results at position 7 near the inner surface. Two peaks are also observed in the azimuthal profile of layer reflection at a small angle (arrows L1 and L2) and mesogenic diffraction at a wide angle (M1 and M2) in Figure 3(7-b). From the peak intensity ratio between peak L1 and peak L2 in Figure 3(7-b), the volume ratio of two smectic domains is estimated to be 1:3, as illustrated in Figure 3(7-c). In a similar manner to the case of position 2 at the second nearest position from the outer surface, the direction of the larger domain due to L1 is found to be almost parallel to the surface of the inside diameter, as illustrated in Figure 3(7-c).

The X-ray results at positions 5 and 6 are shown in Figure 3(5-a)–(5-c),(6-a)–(6-c), respectively. While the azimuthal intensity profiles at positions 5 and 6 in Figure 3(5-b),(6-b), respectively, resemble that at position 7 in Figure 3(7-b), the direction of the X-ray pattern rotates about 20 degrees clockwise from position 5 [Figure 3(5-a)] to position 7 [Figure 3(7-a)]. The molecular orientational models based on the X-ray results at positions 5, 6, and 7 are illustrated in Figure 3(5-c),(6-c),(7-c), respectively.

The molecular alignment models shown in Figure 3(1-c)–(7-c) are combined in Figure 4a to illustrate the cross-section of the elastomer film and discuss the depth profile of molecular alignments. As mentioned above, molecules align uniformly and the direction of the director is almost parallel to the surface in the area of the outer surface at position 1 in Figure 4a. Here, the smectic domain, where the director is parallel to the surface, is tentatively designated as “the parallel domain”. Another domain, where the director inclines at 65 degrees to the director of the parallel domain, appears at position 2, which is a depth of 0.25 mm from the surface. This new domain is designated as “the inclined domain”. The peak intensity ratio between the inclined domain and the parallel domain, which is 1:4 at position 2 (0.25 mm depth), increases as the observed position becomes deeper. It becomes 2:2 (1:1) at position 3 (0.50 mm depth) and then 3:1 at position 4 (0.75 mm depth). In other words, the inclined domain, which does not exist at the surface, becomes larger than the parallel domain at the center position in the cross-sectional profile (0.75 mm depth). In addition, the direction of the domain rotates about 20 degrees clockwise from position 5 to position 7. The director of the larger domain, indicated by L1, at position 7 is almost parallel to the inner surface.



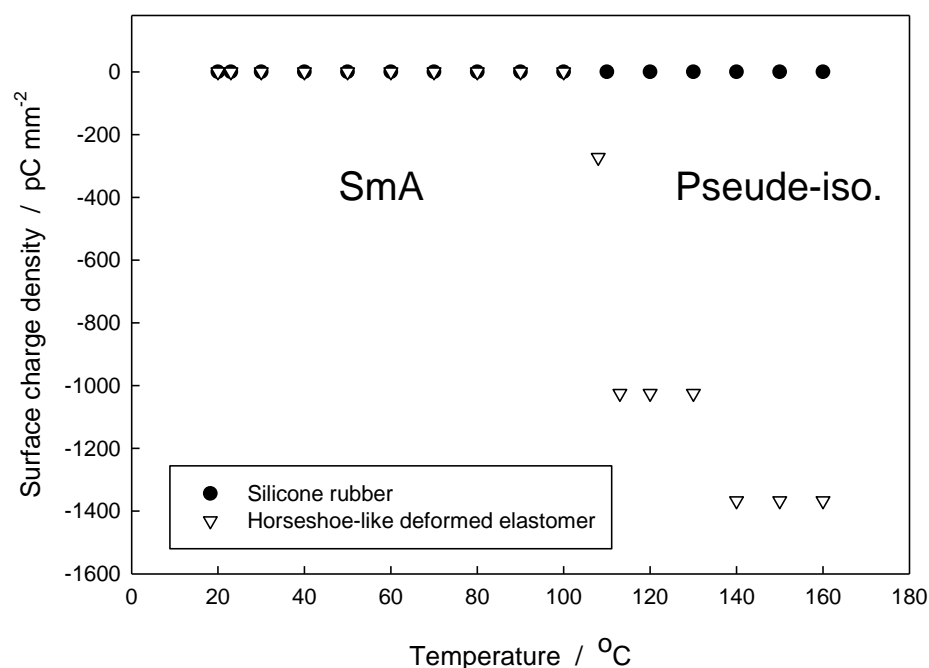
**Figure 4.** Molecular orientation model based on X-ray analysis of the horseshoe-like deformed liquid crystalline elastomer. (a) Schematic model of molecular orientation in cross-section of the liquid crystalline elastomer based on results of X-ray analysis. (b) Hypothetical model of the direction of director in the pseudo-isotropic phase. (c) The flexoelectric polarization due to splay distortion may be locally induced in the pseudo-isotropic phase.

Figure 4b shows a hypothetical model of the direction of local directors in the cross-section of the elastomer in the pseudo-isotropic phase where the orientational order partially remains. The direction of the local director at each position is thought to be governed by the volume ratio of the parallel domain to the inclined domain in the SmA phase. The director is uniformly parallel to the surface at position 1. The director at position 4 is assumed to incline at about 48 degrees ( $=65^\circ \times 3/4$ ) to the director of position 1, as illustrated in Figure 4b, because three-fourths of the area at position 4 corresponds to the domain which inclines 65 degrees relative to the surface. The change in the direction of the local director from position 1 to position 4 seems to induce splay distortion in the pseudo-isotropic phase. Here, splay distortion is defined as a distortion of the director  $n$  expressed by  $(\text{div } n)^2$  [20]. Because the mesogens used here are wedge-shaped, as shown in Figure 1b, the macroscopic polarization  $P_{out} = \sum_{i=1}^4 p_i$  caused by the flexoelectric effect can simultaneously emerge in the horseshoe-like deformed elastomer because the splay distortion is fixed by cross-links, as illustrated in positions 1–4 in Figure 4c [19,20,28].

Subsequently, let us discuss the change in the direction of the local director from position 5 to position 7 shown in Figure 4b. There is almost no change in the ratio of the inclined domain to the parallel domain among positions 5–7, while the direction of the local domain rotates about 20 degrees clockwise from position 5 to position 7. The rotation of the director induces another splay distortion in the pseudo-isotropic phase. The flexoelectric polarization  $P_{in} = \sum_{i=5}^7 p_i$  due to the splay distortion also emerges in the region from position 5 to position 7, as illustrated in Figure 4c.

As the total polarization  $P_{total}$  ( $P_{total} = \sum_{i=1}^7 p_i = \sum_{i=1}^4 p_i + \sum_{i=5}^7 p_i \neq 0$ ) is apparently not canceled out, the macroscopic polarization caused by the flexoelectric effect consequently emerges in the horseshoe-like deformed elastomer in which splay distortion is fixed by cross-links (Figure 4c). The temperature dependence of the surface charge density is measured to confirm the emergence of the polarization in the liquid crystalline elastomer. Two samples are used for investigation: silicone rubber with a thickness of 1.0 mm as the reference sample and the horseshoe-shaped part of the deformed elastomer with splay distortion. Figure 5 shows the temperature dependence of the surface charge density of

these two samples. No electric charge is observed in the temperature region measured between 20 °C and 160 °C in the silicone rubber. Electric charge is also not observed below 100 °C in the horseshoe-shaped part of the deformed elastomer, because the layered structure of the SmA phase disturbs the emergence of splay distortion of the director. An electric charge appears and is estimated to be  $-410 \text{ pC/mm}^2$  at 110 °C in the vicinity of the transition temperature from the SmA phase to the pseudo-isotropic phase. The macroscopic polarization probably emerges because of splay distortion in the pseudo-isotropic phase with the partial orientational order of mesogens.



**Figure 5.** Temperature dependence of surface charge density of two samples: silicone rubber used as a reference sample and the horseshoe-shaped part of deformed elastomer.

Moreover, the surface charge density increases at a temperature above 110 °C. It reaches  $-1367 \text{ pC/mm}^2$  above 140 °C in the temperature region of the pseudo-isotropic phase. In other words, the surface charge density starts to increase in the vicinity of the transition temperature from the SmA phase to the pseudo-isotropic phase, and it reaches  $-1367 \text{ pC/mm}^2$  in the pseudo-isotropic phase in which the splay distortion of the director, due to the remaining orientational order of mesogens, is allowed. As reported in a previous paper [27], the uniaxially deformed liquid crystalline elastomer with uniform orientation of the same mesogens and almost no and/or a small electric charge was observed in the same measured temperature region including the SmA phase as well as the pseudo-isotropic phase, because neither splay nor bend distortion occurred in the uniformly oriented sample. In other words, macroscopic polarization hardly appears in the uniformly aligned liquid crystalline elastomer, in which the dipole moment is macroscopically cancelled out in the symmetric alignment. It may be safely concluded that the splay distortion of wedge-shaped mesogens with a permanent dipole moment is fixed by cross-links in the pseudo-isotropic phase with nematic order and brings about the macroscopic polarization due to flexoelectricity, and that the observed electric charge is caused by the polarization.

#### 4. Conclusions

A liquid crystalline elastomer with wedge-shaped mesogens derived from cholesterol was synthesized with horseshoe-shaped deformation. X-ray diffractometry revealed a cross-sectional profile of the director in the horseshoe-like deformed part of the elastomer in the SmA phase; the director uniformly aligned parallel to the surface in the outer surface area, while it was partially inclined about 65 degrees to the surface inside the

elastomer film. Although no polarization was observed in the SmA phase, the polarization was detected in the pseudo-isotropic phase of the horseshoe-like deformed part of the elastomer. The emergence of polarization suggested that the splay distortion along the depth direction is induced through the transformation from the SmA phase to the pseudo-isotropic phase. The surface charge density due to the polarization increased with the temperature in the pseudo-isotropic phase and reached  $-1367 \text{ pC/mm}^2$ . It was concluded that the macroscopic polarization due to the flexoelectric effect emerged and was fixed in the elastomer within the splay distortion cross-linked in the horseshoe-like deformed liquid crystalline elastomer.

**Author Contributions:** Formal analysis, T.I. and H.M.; Investigation, K.H. and S.T.; Supervision, K.Y. and T.H. All authors have read and agreed to the published version of the manuscript.

**Funding:** This research was supported by a Grant-in-Aid for Scientific Research (C) (#20K05654) from the Ministry of Education, Culture, Sports, Science and Technology (MEXT).

**Institutional Review Board Statement:** Not applicable.

**Informed Consent Statement:** Not applicable.

**Data Availability Statement:** Not applicable.

**Acknowledgments:** We would like to thank Syunta Asada and Naoki Shimura for valuable discussions.

**Conflicts of Interest:** The authors declare no conflict of interest.

## References

1. Finkelmann, H.; Kock, H.J.; Rehage, G. Liquid crystalline elastomers—A new type of liquid crystalline material. *Makromol. Chem. Rapid Commun.* **1981**, *2*, 317–322. [[CrossRef](#)]
2. Zentel, R. Liquid crystalline elastomers. *Angew. Chem. Adv. Mater.* **1989**, *101*, 1437–1445. [[CrossRef](#)]
3. Brand, H.R.; Finkelmann, H. Physical properties of liquid crystalline elastomers. In *Handbook of Liquid Crystals*; Demus, D., Goodby, J., Gray, G.W., Spiess, H.W., Vill, V., Eds.; Wiley-VCH: Weinheim, Germany, 1989; Volume 3, pp. 277–302.
4. Warner, M.; Terentjev, E.M. *Liquid Crystal Elastomers*; Revised Edition; Clarendon Press: Oxford, UK, 2007; pp. 1–46.
5. De Gennes, P.G. Un muscle artificiel semi-rapide. *C. R. Acad. Sci.* **1997**, *324*, 343–348. [[CrossRef](#)]
6. Neufeld, R.A.E.; Shahsavan, H.; Zhao, B.X.; Abukhdeir, N.M. Simulation-based design of thermally-driven actuators using liquid crystal elastomers. *Liq. Cryst.* **2018**, *45*, 1010–1022. [[CrossRef](#)]
7. Skačej, G. Elastocaloric effect in liquid crystal elastomers from molecular simulations. *Liq. Cryst.* **2018**, *45*, 1964–1969. [[CrossRef](#)]
8. Ube, T.; Yoda, T.; Ikeda, T. Fabrication of photomobile polymer materials with phase-separated structure of crosslinked azobenzene liquid-crystalline polymer and poly(dimethylsiloxane). *Liq. Cryst.* **2018**, *45*, 2269–2273. [[CrossRef](#)]
9. Braun, L.B.; Zentel, R. Functional liquid crystalline particles and beyond. *Liq. Cryst.* **2019**, *46*, 2023–2041. [[CrossRef](#)]
10. Lehmann, W.; Skulpin, H.; Tolksdorf, C.; Gebhard, E.; Zentel, R.; Krüger, P.; Lösche, M.; Kremer, F. Giant lateral electrostriction in ferroelectric liquid-crystalline elastomers. *Nature* **2001**, *410*, 447–450. [[CrossRef](#)]
11. Köhler, R.; Stannarius, R.; Tolksdorf, C.; Zentel, R. Electroclinic effect in free-standing smectic elastomer films. *Appl. Phys. A* **2005**, *80*, 381–388. [[CrossRef](#)]
12. Spillmann, C.M.; Ratna, B.R.; Naciri, J. Anisotropic actuation in electroclinic liquid crystal elastomers. *Appl. Phys. Lett.* **2007**, *90*, 021911. [[CrossRef](#)]
13. Spillmann, C.M.; Kapur, A.V.; Bentrem, F.W.; Naciri, J.; Ratna, B.R. Critical field strength in an electroclinic liquid crystal elastomer. *Phys. Rev. Lett.* **2010**, *104*, 227802. [[CrossRef](#)]
14. Eckert, T.; Finkelmann, H. Piezoelectricity of mechanically oriented Sc\*-elastomers. *Macromol. Rapid Commun.* **1996**, *17*, 767–773. [[CrossRef](#)]
15. Adams, J.M.; Warner, M.; Stenull, O.; Lubensky, T.C. Smectic-A elastomers with weak director anchoring. *Phys. Rev. E* **2008**, *78*, 011703. [[CrossRef](#)] [[PubMed](#)]
16. Hiraoka, K.; Stein, P.; Finkelmann, H. Electromechanics of a chiral smectic C elastomer: Measurement of complex piezoelectric constant through successive phase transformation. *Macromol. Chem. Phys.* **2004**, *205*, 48–54. [[CrossRef](#)]
17. Hiraoka, K.; Kobayashi, M.; Kazama, R.; Finkelmann, H. Electromechanics of monodomain chiral smectic C elastomer: Mechanical response to electric stimulation. *Macromolecules* **2009**, *42*, 5600–5604. [[CrossRef](#)]
18. Hiraoka, K.; Kishimoto, T.; Kato, M.; Tashiro, T. Electroclinic and electromechanical effects of a side-chain chiral smectic A elastomer. *Liq. Cryst.* **2011**, *38*, 489–493. [[CrossRef](#)]
19. Meyer, R.B. Piezoelectric effects in liquid crystals. *Phys. Rev. Lett.* **1969**, *22*, 918–921. [[CrossRef](#)]
20. De Gennes, P.G.; Prost, J. *The Physics of Liquid Crystals*, 2nd ed.; Oxford Science Publications: Oxford, UK, 1993; pp. 10–20, 135–139.
21. Patel, J.S.; Meyer, R.B. Flexoelectric electro-optics of a cholesteric liquid crystal. *Phys. Rev. Lett.* **1987**, *58*, 1538–1540. [[CrossRef](#)]

22. Rudquist, P.; Komitov, L.; Lagerwall, S.T. Linear electro-optic effect in a cholesteric liquid crystal. *Phys. Rev. E* **1994**, *50*, 4735. [[CrossRef](#)]
23. Popova, E.V.; Kopeychenko, E.I.; Krivoshey, V.V.; Fedoryako, A.P. Piezoelectric and flexoelectric effects in ferroelectric liquid crystals. *Phys. Rev. E* **2012**, *86*, 031705. [[CrossRef](#)]
24. Meyer, C.; Luckhurst, G.R.; Dozov, I. Flexoelectrically driven electroclinic effect in the twist-bend nematic phase of achiral molecules with bent shapes. *Phys. Rev. Lett.* **2013**, *111*, 067801. [[CrossRef](#)] [[PubMed](#)]
25. Sreenilayam, S.; Panarin, Y.; Vij, J.K.; Torgova, S.I.; Lehmann, A.; Tchierske, C. Flexoelectric polarization studies in bent-core nematic liquid crystals. *Phys. Rev. E* **2015**, *92*, 022502. [[CrossRef](#)] [[PubMed](#)]
26. Harden, J.; Chambers, M.; Verduzco, R.; Luchette, P.; Gleeson, J.T.; Sprunt, S.; Jakli, A. Giant flexoelectricity in bent-core nematic liquid crystal elastomers. *Appl. Phys. Lett.* **2010**, *96*, 102907. [[CrossRef](#)]
27. Hiraoka, K.; Ishihara, T.; Minami, H.; Taira, S.; Komesu, S.; Yamada, K.; Oshima, M. Spontaneous polarization due to flexoelectric effect in liquid crystalline elastomers prepared by cross-linking under splay distortion. *Liq. Cryst.* **2022**, *49*, 2051–2057. [[CrossRef](#)]
28. Hiraoka, K.; Kashimura, H.; Tanaka, S.; Kaneshima, S. Electric-field-induced deformation of chiral smectic A liquid-crystalline elastomers composed of cholesterol derivative mesogens. *Mol. Cryst. Liq. Cryst.* **2017**, *646*, 168–175. [[CrossRef](#)]
29. Hiraoka, K.; Taira, S.; Hoshino, Y.; Ishihara, T.; Yamada, K.; Oshima, M. Electric-field-induced deformation caused by electroclinic and flexoelectric effects in liquid-crystalline elastomer with wedge-shaped mesogens derived from cholesterol. *Liq. Cryst.* **2021**, *47*, 1535–1545. [[CrossRef](#)]
30. Frisch, M.J.; Trucks, G.W.; Schlegel, H.B.; Scuseria, G.E.; Robb, M.A.; Cheeseman, J.R.; Scalmani, G.; Barone, V.; Petersson, G.A.; Nakatsuji, H.; et al. *Gaussian 16, Revision B.01*; Gaussian, Inc.: Wallingford, CT, USA, 2016.
31. Hiraoka, K.; Tagawa, N.; Baba, K. Shape-Memory effect controlled by the crosslinking topology in uniaxially-deformed smectic C\* elastomers. *Macromol. Chem. Phys.* **2008**, *209*, 298–307. [[CrossRef](#)]
32. Rössle, M.; Braun, L.; Schollmeyer, D.; Zentel, R.; Lagerwall, J.P.F.; Giesselmann, F.; Stannarius, R. Differences between smectic homo- and co-polysiloxanes as a consequence of microphase separation. *Liq. Cryst.* **2005**, *32*, 533–538. [[CrossRef](#)]
33. Mitchell, G.R.; Windle, A.H. Orientation in liquid crystal polymers. In *Developments in Crystalline Polymers-2*; Bassett, D.C., Ed.; Elsevier Applied Science: Essex, UK, 1988; Chapter 3.

**Disclaimer/Publisher's Note:** The statements, opinions and data contained in all publications are solely those of the individual author(s) and contributor(s) and not of MDPI and/or the editor(s). MDPI and/or the editor(s) disclaim responsibility for any injury to people or property resulting from any ideas, methods, instructions or products referred to in the content.